Electrical Power and Energy Systems 155 (2024) 109541

Contents lists available at ScienceDirect

International Journal of Electrical Power and Energy Systems

journal homepage: www.elsevier.com/locate/ijepes

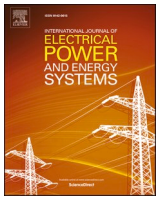

# Faulted phase selection multicriteria algorithm implemented in generic hardware for centralized P&C in smart grids

María Teresa Villén Martínez [a,*], Maria Paz Comech [b], Anibal Antonio Prada Hurtado [a], Miguel Angel Olivan [a], Carlos Rodriguez del Castillo [c], David López Cortón [d], Rubén Andrino Gallego [d]

[a] Power System Protection Team (Infrastructure of Electric Grids Group), Fundacion CIRCE, Zaragoza, Spain
[b] Instituto Universitario de Investigación CIRCE (Fundación CIRCE—Universidad de Zaragoza), Zaragoza, Spain
[c] Elewit (A Company of Redeia), Madrid, Spain
[d] Red Eléctrica (A Company of Redeia), Madrid, Spain

ARTICLE INFO

*Keywords:*
Protection relays
Faulted phase selector
Distance protection
Digital substation

ABSTRACT

The integration of devices based on renewable energies and power electronics makes it necessary to rethink some of the methods used for protection and control in distribution and transmission grids. The difference between short circuit current contributions from renewable and conventional generators may affect protection system operation. Fault phase selection is one of the elements to be analyzed under renewable generation scenarios due to its importance in protection functions such as distance protection.

The digitization of substations presents new opportunities in control and protection systems, such as functionality increase, reliability improvement, cost reduction of the installation and capacity for remote maintenance. This paper proposes a multi-criteria fault phase selection algorithm developed to be implemented in digital substations. The proposed faulted phase algorithm combines the results provided by four independent protection algorithms and has been designed to be applied in transmission power systems. Depending on the electrical variables measured in each event, quality criteria are defined to consider the strengths and weaknesses of each independent algorithm. The proposed algorithm has been implemented and tested on the centralized protection and control platform called EPICS, obtaining very satisfactory results.

## 1. Introduction

The main function of protection devices in electrical power systems is to detect disturbances and isolate them as quickly as possible to ensure safety and system stability and maintain the quality and security of the supply. Different protection devices are installed in the electrical network to protect it against faults, and one of the most used is distance protection [1]. This protection function requires to calculate correctly the apparent impedance and to identify the direction of the fault and the phases involved to operate appropriately.

Different algorithms have been proposed in the literature to determine the phases involved during a fault [2–15]. These algorithms aim to provide new solutions that overcome the issues found by faulted phase selectors during their operation in the electric power system. In [16] an algorithm to select the ground fault phase under weak infeed conditions is proposed. The presented algorithm combines the frequency components and superimposed values to carry out this selection. The solution from [3] is based on the correlation of transient voltage to perform the phase selection. This approach is valid for the protection relays of wind power plants. The phase selection in [4] is based on impedance measurement and uses the residual current compensation development. The approach described in [5] is based on the adaptive cumulative sum method (ACUSUM) to detect faults and discriminate faulted phases in transmission lines. Two faulted phase selection logics are exposed in [6], one based on superimposed currents and the other on sequence voltage. The algorithm based on sequence-current shown in [7] considers the fault resistance and the element with the lowest calculated reach to select single line-to-ground and line-to-line faults. In [8], a solution based on the initial current travelling wave is developed. The phase selector proposed in [9] uses superimposed sequence components and correlation analysis to carry out the phase selection. The faulted phase selector in [10] improves the behavior, and is based on sequence components during power swing. The phase selector described

* Corresponding author.
*E-mail address:* mtvillen@fcirce.es (M.T. Villén Martínez).

https://doi.org/10.1016/j.ijepes.2023.109541
Received 22 March 2023; Received in revised form 21 July 2023; Accepted 27 September 2023
Available online 6 October 2023

**Nomenclature**

| | |
|---|---|
| EPICS | Edge Protection and Intelligent Control System |
| FP | Faulted Phase |
| FPS | Faulted Phase selection |
| FPSA | Faulted Phase selection algorithm |
| GTNET | Giga-transceiver network communication |
| HiL | Hardware in the Loop |
| $I_{A1}$ | Positive sequence current |
| $I_{A2}$ | Negative sequence current |
| $I_{A0}$ | Zero-sequence current |
| $k_i$ and $\beta_{Mi}$ | Design parameters |
| M-FPSA | Multicriteria Faulted Phase selection algorithm |
| MU | Merging Unit |
| $Q_i$ | Quality Factor |
| PV | Photovoltaic power plant |
| RTDS | Real time digital simulator |
| SIR | Source impedance ratio |
| SV-APM | Sampled Values based Analog Processing Module |
| $V_{A1}$ | Positive sequence voltage |
| $V_{A2}$ | Negative sequence voltage |
| $V_{A0K}$ | Zero-sequence voltage |
| $\Delta I_A$, $\Delta I_B$, $\Delta I_C$ | Sampled single line current variations |
| $\Delta I_{AB}$, $\Delta I_{BC}$, $\Delta I_{CA}$ | Sampled line to line current variations |
| $\Delta V_{AN}$, $\Delta V_{BN}$, $\Delta V_{CN}$ | Sampled single line-to-ground voltage variations |
| $\Delta V_{AB}$, $\Delta V_{BC}$, $\Delta V_{CA}$ | Sampled line-to-line voltage variations |

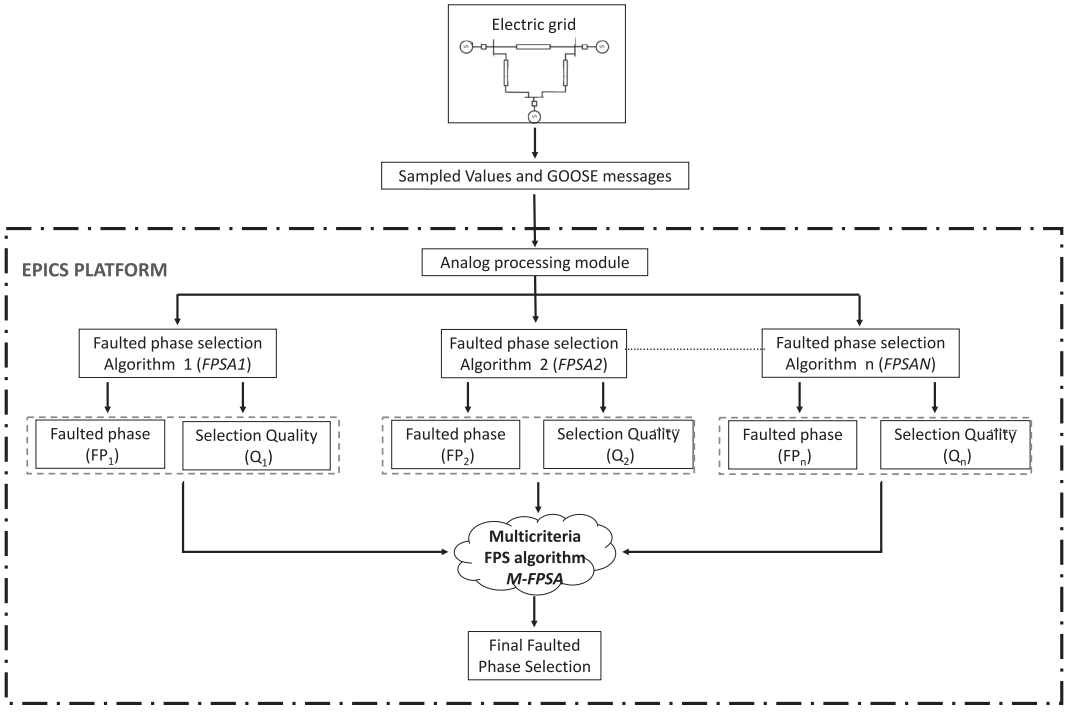


**Fig. 1.** General Flowchart of the methodology used during the study.

in [11] uses artificial neural networks. The algorithm from [12] determines the fault type using superimposed and steady-state components of fault voltage. The solution described in [13] is based on sequence components to identify the faulted phase of high-resistance ground faults. The faulted phase algorithm described in [14] is focused on phasors to select the faulted phase in ultra-high voltage transmission lines. The faulted phase selector described in [15] uses a method based on transient components to carry out the faulted phase selection in double-circuit transmission lines.

However, the solutions listed above are valid for the specific cases presented in each paper but not for the rest of the possible scenarios. For example, [16] proposes an algorithm to select ground faulted phase under weak infeed conditions and [5] develops a faulted phase algorithm that can be applied in double circuit transmission lines and allow discriminating faulted phases within 1 ms after fault detection. Nevertheless, these algorithms are not tested in other possible scenarios. Therefore, it is relevant to implement, debug, and check these different algorithms using a platform that allows simulating power system operation scenarios to study the behavior in such scenarios.

The EPICS Platform (Edge Protection and Intelligent Control System) [17] was developed to create a flexible, scalable, replicable, manageable, and cyber secure hardware and software platform to be used in very different application environments (transmission, distribution, industry, …). EPICS allow implementing architectures based on containerized microservices, such as differential and distance protection, that can be executed on generic hardware making software independent from hardware. EPICS can be used as a centralized protection system in digital substations. Besides, it enables the development of new protections, controls, and monitoring algorithms in generic hardware to be tested in the laboratory.

Consequently, this study proposes a novel Multicriteria Faulted Phase Selection Algorithm (*M-FPSA*) applicable to transmission power systems that improves the results obtained by algorithms usually implemented in commercial protection relays for a wide range of electric power system operating conditions. This paper initially assesses the performance of four faulted phase selection algorithms. Two of these algorithms are proposed and developed during this study. These two algorithms are based on the superimposed components theory; the first

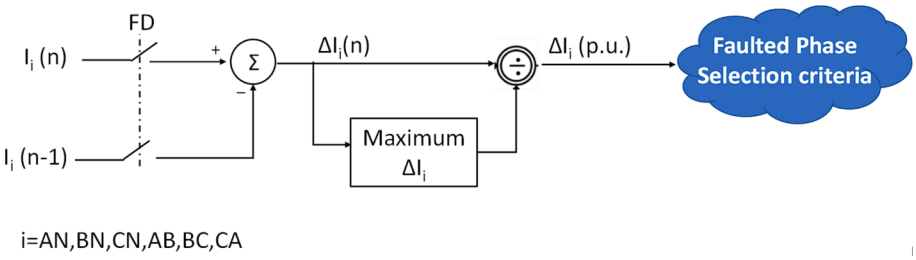


**Fig. 2.** Scheme of Faulted phase selection algorithm based on Superimposed Sequence Currents.

employs superimposed sequence currents, and the second uses superimposed sequence voltages to perform the faulted phase selection. The rest of the algorithms are selected and adapted from the literature review. These algorithms are based on frequency domain components and select the faulted phase using sequence voltages [6] and sequence currents [7].

Once the algorithms are defined, they are implemented, containerized and added to the EPICS platform as microservices [17]. The behavior of these algorithms is tested in different scenarios based on real electric grids, considering conventional and unconventional sources, and strong and weak grids. After the evaluation, a multicriteria faulted phase selector is proposed and tested using the same scenarios.

A Hardware-in-the-Loop (HiL) configuration with a Real-Time Digital Simulator (RTDS) [18] is used to carry out the tests. In HiL, RTDS reproduces events that can appear in an electric power system modelled in RSCAD software, generating currents and voltages seen by the relay during a fault and recording the relay behavior. Examples of RTDS test applications can be found in [19–22]. In this study, RTDS publishes and subscribes sampled values using IEC 61850-9-2 LE profile [23] and GOOSE messages using IEC 61850-8-1. The multicriteria faulted phase selector implemented in the EPICS platform uses this information to provide a final faulted phase selection.

To describe the developed work, the paper is structured as follows. Section 2 describes the general methodology used during the faulted phase selection study. The four faulted phase selection algorithms used to assess faulted phase selection are described in Section 3. After that, Section 4 describes the quality criteria proposed in this study to provide reliability to the faulted phase selection. The criterion used to obtain a final faulted phase selection is also described. The laboratory test bench and the test network used to evaluate the Multicriteria Faulted Phase Selector is described in Section 5 and Section 6. Finally, the main results and conclusions are included in Sections 7 and 8.

## 2. General methodology description

The methodology flowchart used during the faulted phase selection is described in Fig. 1.

In the electric grid from the top of the figure, instrument transformers (current and voltage transformers) measure the primary currents and voltages analog signals, and the Merging unit (MU) converts and merges these signals into digital messages, which are published according to IEC 61850-9 LE standard [23] and via Ethernet multicast.

EPICS platform subscribes and processes these data through the "Sampled Values based Analog Processing Module" (SV-APM) implemented in a platform of generic hardware, and, after that, the signals can be used by the protection functions implemented in the platform, among which is the novel multicriteria faulted phase selection algorithm (*M-FPSA*) developed in this research.

The *M-FPSA* proposed is described within the dashed line box in Fig. 1, which is based on the combination of different faulted phase selection algorithms (*FPSA1*, *FPSA2*, …, *FPSAn*) to obtain the final result. In this work, four algorithms have been implemented: two based on the literature, and the other two proposed and developed during this study. Each algorithm obtains a result for the faulted phase ($FP_1$, $FP_2$, …, $FP_n$), and the *M-FPSA* applies to them a quality factor ($Q_1$, $Q_2$, …, $Q_n$) whose definition has been determined in this work based on extensive simulations in multiple power system conditions. These factors represent the strength and reliability of the faulted phase selection made by each algorithm; the higher the quality factor, the more reliable the faulted phase selection provided by the algorithm is.

Once phase selections ($FP_i$) and quality factors ($Q_i$) are obtained, they are combined by the *M-FPSA* to get the final faulted phase selection result.

All in all, to implement and test this methodology, three steps must be followed:

- Step 1. Select the faulted phase selection algorithms whose outputs will be combined later by the *M-FPSA*.
- Step 2. Definition of the weight criteria used for calculating the quality to be considered by the *M-FPSA*.
- Step 3. Use the *M-FPSA* for the optimal combination of the outputs of the faulted phase selection algorithms, which will result in a final faulted phase selection.

## 3. Faulted phase selection algorithms

As indicated in the previous Section 2, the proposed *M-FPSA* is based on combining several FPS algorithms. This section describes the *FPSA1* and *FPSA2,* proposed and developed during this study, and *FPSA3* and *FPSA4*, which are based on the literature review.

### 3.1. Faulted phase selectors proposed during this study

#### 3.1.1. FPSA1: Faulted phase selector based on superimposed sequence currents

The principle of this technique is based on the variation between current (or voltage) signal before and during a disturbance. To obtain these variations, the phasor current (or voltage) measured one or two cycles before the disturbance is subtracted from the transient signal after a disturbance or fault inception [24,25]. The resulting signal obtained from applying this technique is known as superimposed sequence quantity. After a complete cycle, when steady fault conditions are reached, the superimposed sequence quantities value disappears.

The superimposed sequence quantities technique has several advantages, such as not needing any settings, allowing the phases involved during a fault to be selected very quickly and increasing the sensitivity due to pre-fault conditions are removed from the signal [12,26]. By contrast, in scenarios where fault conditions are similar to pre-fault values or slow evolving faults, this technique can provide wrong results [6].

Fig. 2 shows the scheme of *FPSA1,* which uses the module both the sampled single line current variations ($\Delta I_A$, $\Delta I_B$, $\Delta I_C$) and sampled line to line current variations ($\Delta I_{AB}$, $\Delta I_{BC}$, $\Delta I_{CA}$) for the operation of the proposed FPSA.

As it is shown in Fig. 2, when the fault detector signal (*FD*) is activated, the proposed algorithm calculates the current variations ($\Delta I_i(n)$)

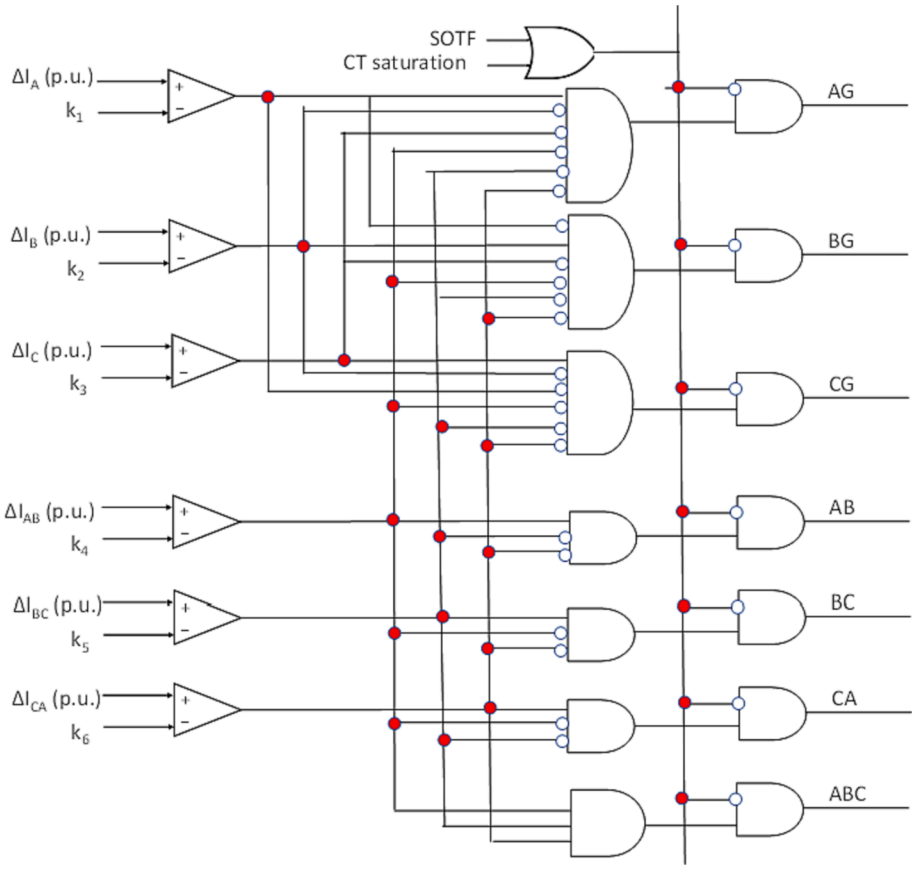


**Fig. 3.** *FPSA1* criteria based on Superimposed Sequence Currents.

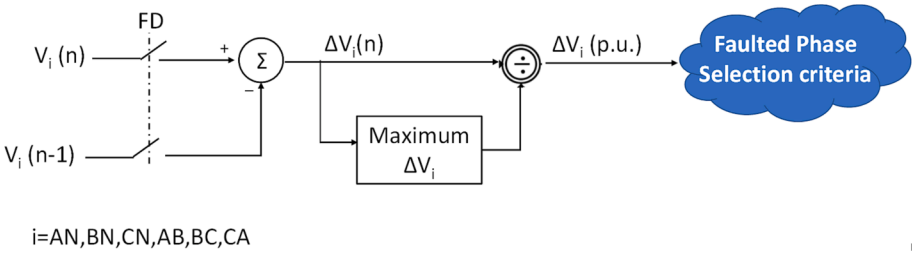


**Fig. 4.** Scheme of Faulted phase selection algorithm based on Superimposed Sequence Voltages.

using the sampled phase currents phasor measured in the present timestamp ($I_i(n)$) and the measured in a previous complete cycle ($Ii(n-1)$). The prefault current phasors measured one full cycle before the fault detector activation are stored and used by *FPSA1* during the faulted phase selection. Once these current variations are calculated, the maximum variation is identified and used as the base to obtain the per unit current variations ($\Delta I_i$ *(p.u.)*). The faulted phase selection criteria compare the module of $\Delta I_i$ *(p.u.)* with several thresholds experimentally obtained (design parameters from $k_1$ to $k_6$) to decide the phases involved during a fault, as is depicted in Fig. 3.

Although the implemented algorithm has several advantages, such as the quick selection of the phases involved during the fault, high sensitivity during algorithm operation or the ability to detect evolving faults and open pole scenarios, it has some limitations. For example, in the case of detection of current transformer saturation, the current measurements used by the algorithm are not reliable and therefore, the algorithm operation must be blocked. Furthermore, when a switch-on-to-fault (SOTF) happens, due to the lack of current measurements in the previous complete cycle, the reliability of the faulted phase provided by the algorithm must be penalized. These limitations highlight the need to combine the algorithm with others to provide a reliable faulted phase selection in most parts of grid operation.

### 3.1.2. FPSA2: Faulted phase selector based on superimposed sequence voltages

*FPSA2* uses both the sampled single line-to-ground voltage variations ($\Delta V_{AN}$, $\Delta V_{BN}$, $\Delta V_{CN}$) and sampled line-to-line voltage variations ($\Delta V_{AB}$, $\Delta V_{BC}$, $\Delta V_{CA}$) for its operation. Fig. 4 shows the scheme of this FPSA:

As it is shown in Fig. 4, when the fault detector signal (*FD*) is activated, the proposed algorithm calculates the voltage variations ($\Delta V_i(n)$) using the sampled phase-to-ground and line-to-line voltage phasors measured in the present timestamp ($V_i(n)$) and the ones measured in a previous full cycle ($V_i(n-1)$). Once these voltage variations are calculated, the maximum variation is identified and used as the base to obtain the per unit voltage variations ($\Delta V_i$ *(p.u.)*). The faulted phase selection criteria compare the module of $\Delta V_i$ *(p.u.)* with several thresholds experimentally obtained (design parameters from $k_1$ to $k_6$) to decide the phases involved during a fault, as it is depicted in Fig. 5 are used.

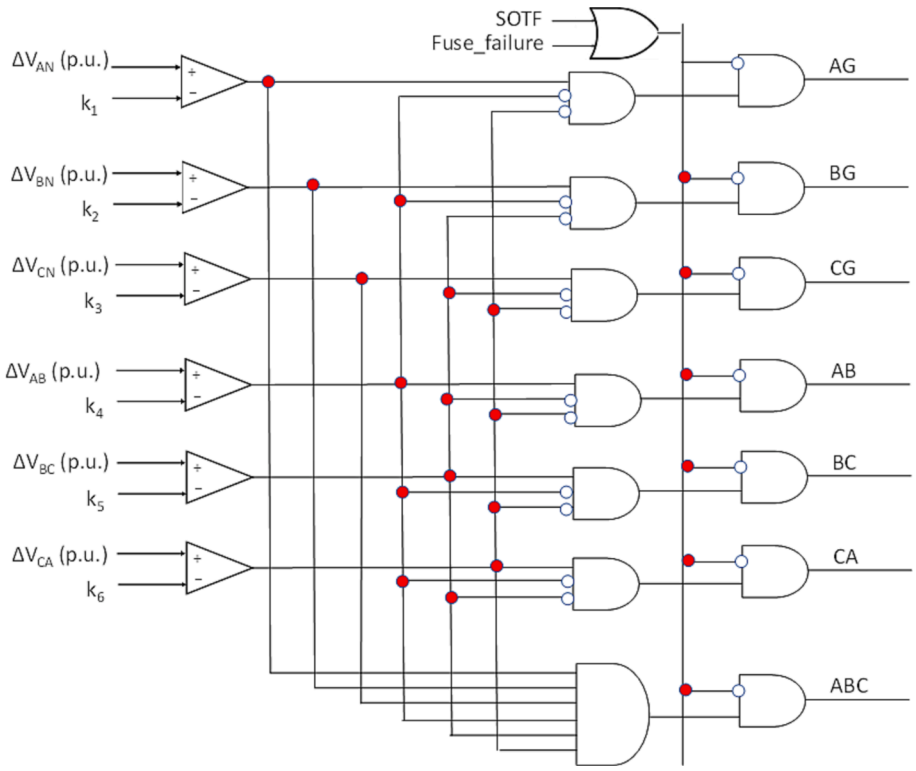


**Fig. 5.** FPSA2 criteria based on Superimposed Sequence Voltages.

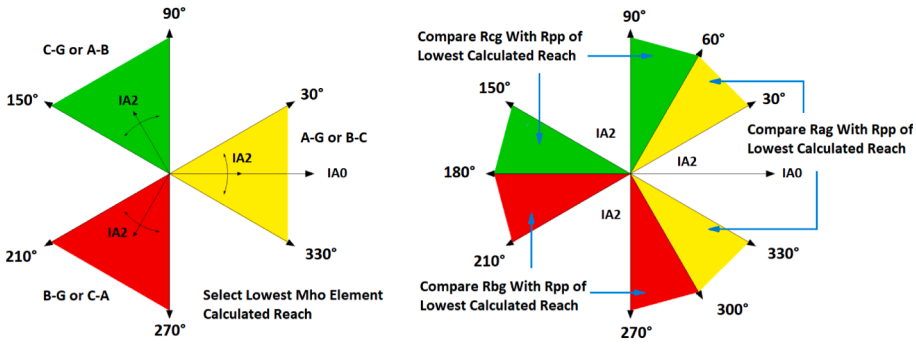


**Fig. 6.** Graphical representation of FID operation [7] (a) Sector angle when resistive faults that $I_{A2}$ angle fall inside the sectors (b) Sector angle when the resistive cause that $I_{A2}$ angle falls outside the sectors showed in (a).

Although the implemented algorithm has several advantages, such as the quick selection of the phases involved during the fault, high sensitivity during algorithm operation or the ability to detect open pole scenarios, it has some limitations. For example, in case of detection of fuse failure, voltage measurements are unreliable; consequently, the algorithm operation must be blocked. voltage measurements are taken from the line side, due to the lack of voltage measurements in the previous complete cycle, the reliability Furthermore, in the case of SOTF, when the of the faulted phase provided by the algorithm must be penalized. These limitations highlight the need to combine the algorithm with others to provide a reliable faulted phase selection in near all cases of grid operation.

### 3.2. Faulted phase selection algorithms based on literature review

#### 3.2.1. FPSA3: Faulted phase selector based on sequence currents and impedance measurement

*FPSA3* is based on the fault identification selection logic (*FID*) described in [7]. It considers the phase angle difference between negative sequence current ($I_{A2}$) and zero-sequence current ($I_{A0}$) and the reach of the element to select the faulted loop. Following figure shows a graphical representation of the faulted phase selector algorithm operation:

Fig. 6(a) represents the phase shift between $I_{A2}$ and $I_{A0}$ for the different fault types. The fault type can be AG or BCG if phase shift is 0°, with a phase margin of ±30° (yellow sector). The final fault type selection between AG or BCG will be based on the lowest calculated reach for these elements. The fault type can be either BG or CAG if $I_{A2}$ lags $I_{A0}$ by 120°, with a phase margin of ±30° (red sector), finally selecting the

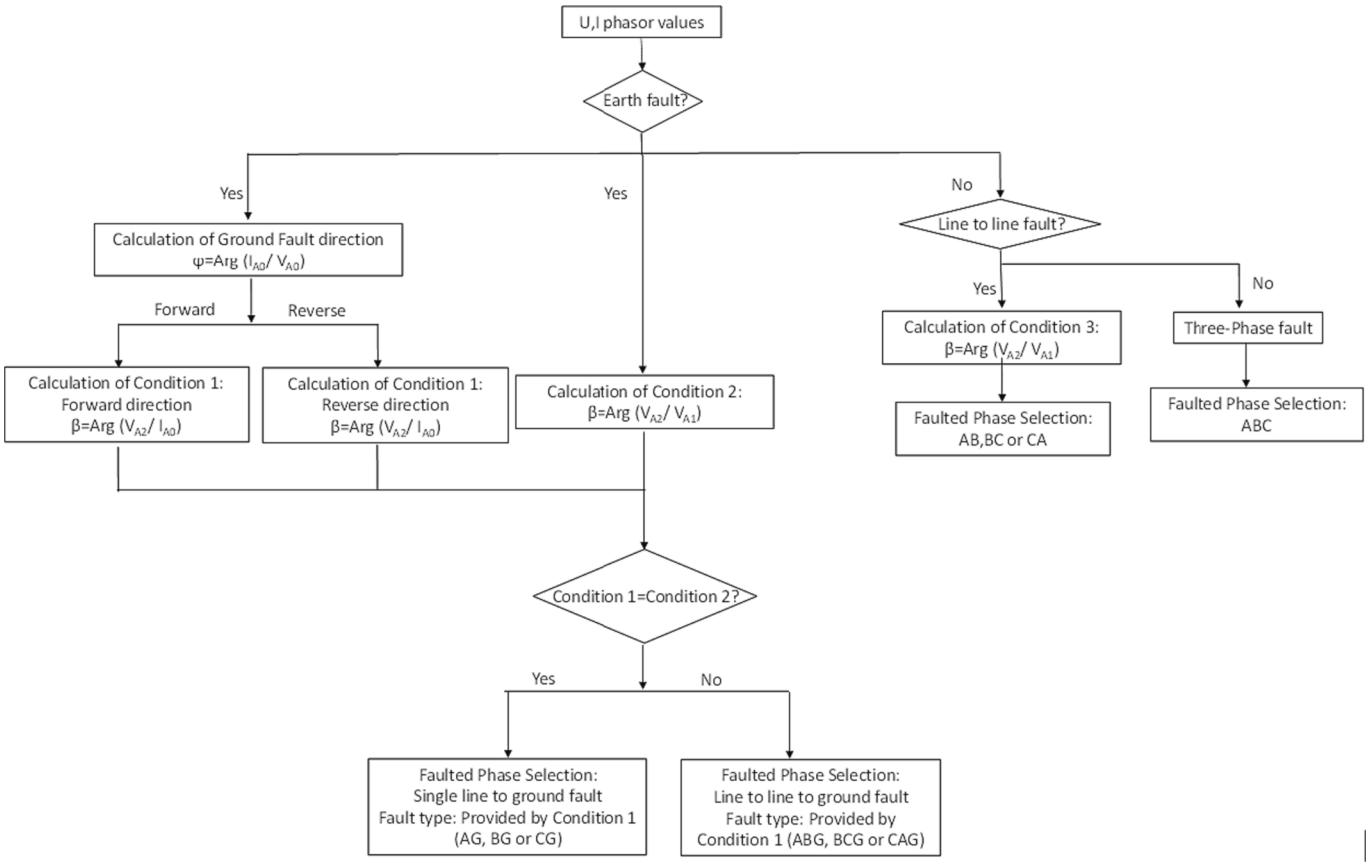


**Fig. 7.** FPSA4 flowchart.

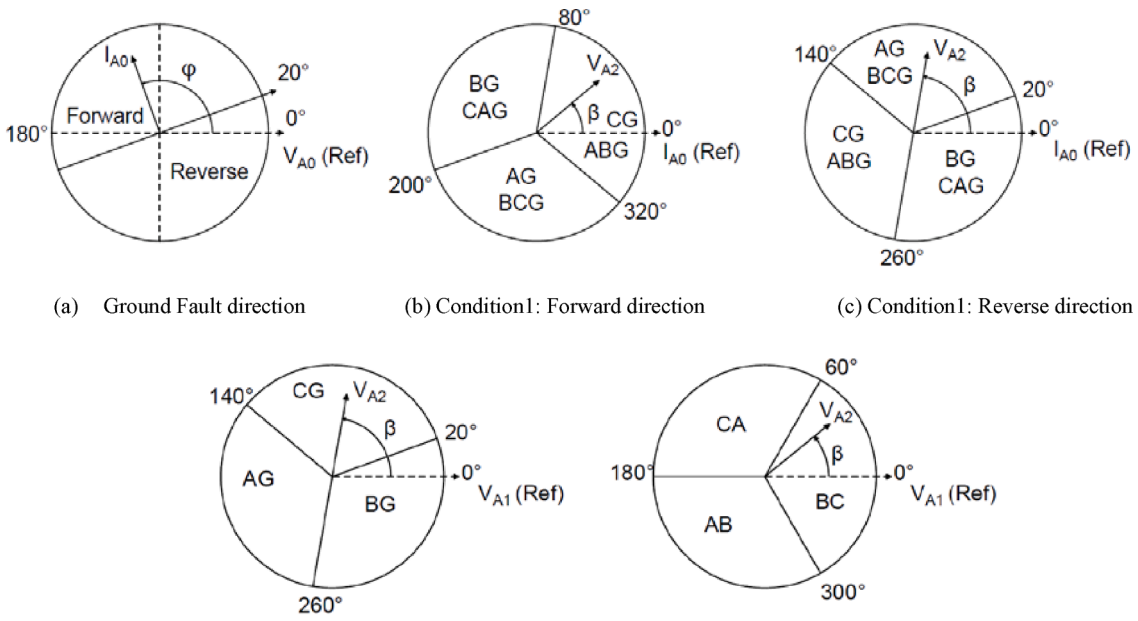


(a) Ground Fault direction (b) Condition1: Forward direction (c) Condition1: Reverse direction

(d) Ground fault Condition 2 (e) Line to line fault Condition 3

**Fig. 8.** Details of the conditions to be used in the flowchart described in Fig. 7.

loop with the lowest calculated reach. Finally, if $I_{A2}$ leads $I_{A0}$ by 120°, with a phase margin of ±30° (green sector), the fault type can be either CG or ABG, selecting the loop with the lowest calculated reach.

In resistive grounded faults, the phase shift between $I_{A2}$ and $I_{A0}$ increases and can cause it to fall outside the angular sectors described in Fig. 6(a). In this scenario, Fig. 6(b) is used to identify the fault type. If $I_{A2}$ fall inside the angular sector [30°−60°] or [300°−330°] (yellow sector), the AG fault resistance ($R_{AG}$) is calculated and compared with the fault

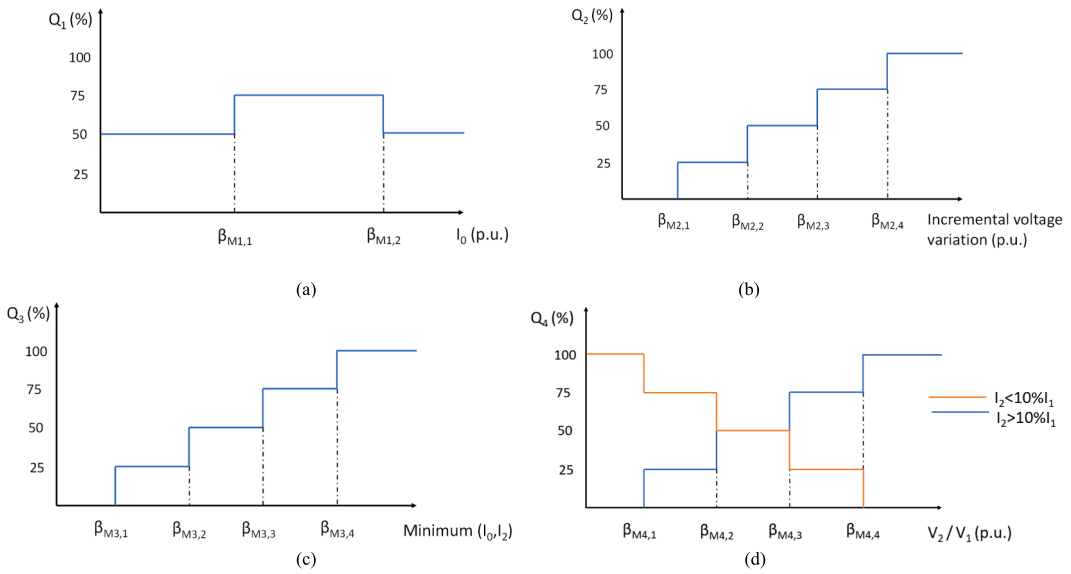


**Fig. 9.** Faulted Phase Selection Quality depending on the algorithm: (a) *FPSA1* quality criterion; (b) *FPSA*2 quality criterion; (c) *FPSA*3 quality criterion; (d) *FPSA*4 quality criterion.

resistance of the phase-to-phase loop ($R_F$) with the lowest calculated reach, selecting AG loop in case of $R_{AG}$ is lower than $R_F$, or the loop with minimum reach in case of $R_{AG}$ is higher than $R_F$. By contrast, when $I_{A2}$ fall inside the angular sector [60°–90°] or [150°–180°] (green sector), the BG fault resistance ($R_{BG}$) is calculated and compared with the $R_F$, selecting the BG loop in case of $R_{BG}$ is lower than $R_F$, or the loop with minimum reach in case of $R_{BG}$ is higher than $R_F$. Finally, when $I_{A2}$ fall inside the angular sector [180°–210°] or [270°–300°] (red sector), the CG fault resistance ($R_{CG}$) is calculated and compared with the $R_F$, selecting the CG loop in case of $R_{CG}$ is lower than $R_F$, or the loop with minimum reach in case of $R_{CG}$ is higher than $R_F$.

It should be noticed that the described algorithm has a significant limitation. It focuses only on fault scenarios involving ground connection, so double-line or three-phase faults cannot be identified. Furthermore, as in *FPSA1*, the algorithm operation must be blocked in case of current transformer saturation. Consequently, the algorithm must be combined with others to identify the phases involved for all fault types.

### 3.2.2. *FPSA4: Faulted phase selector based on sequence voltages*

*FPSA4* is based on voltage phasors and is described in [6]. This algorithm performs the faulted phase identification by evaluating the angle relationship between negative sequence voltage ($V_{A2}$) and positive sequence voltages ($V_{A1}$), and between zero-sequence voltage ($V_{A0}$) and zero-sequence current ($I_{A0}$). The following figure summarizes the flowchart used by the algorithm.

As described in Fig. 7, the algorithm initially checks if the fault can be classified as an "Earth fault" by comparing the negative and zero-sequence voltages and currents with their respective thresholds. If thresholds are exceeded, a single line-to-ground or double line-to-ground fault will be selected (see Fig. 8).

The following steps allow for distinguishing the phase or phases involved during the fault. First, the algorithm needs to identify the fault direction. Considering the phase shift between $I_{A0}$ and $V_{A0}$ *and* taking $V_{A0}$ *as reference*, the fault will be classified as a "*Forward fault*" ($I_{A0}$ angle varies in the range from 20° to 200°) or "*Reverse fault*" ($I_{A0}$ angle ranges from 200° to 20°). Depending on the fault direction, the angle sectors used to check "*Condition 1*", differs 180°. In "*Condition 1*", the phase shift between $V_{A2}$ and $I_{A0}$ is calculated, and an initial faulted phase identification is carried out. For example, if a forward fault is identified in the previous step and $V_{A2}$ is in phase with $I_{A0}$ ($\beta = 0°$), "*Condition 1*" establishes that the fault can be classified as CG or ABG.

The evaluation of "*Condition 2*" is also needed to perform a final identification. "*Condition 2*" selects the fault type based on the phase displacement between $V_{A2}$ and $V_{A1}$, and depending on this phase shift, an AG, BG or CG fault is identified. A final faulted phase selection is performed using faulted phase selections provided by "*Condition 1*" and "*Condition 2*". If both conditions give the same faulted phase identification, a single line-to-ground fault occurs in the phase provided by "*Condition 1*". For example, suppose a CG and ABG fault is identified from "*Condition 1*", and a CG fault is selected from "*Condition 2*". In that case, algorithm provides a CG fault in the faulted phase identification. By contrast, if both conditions differ from the faulted phase identification point of view, a double line to ground fault in the phases provided by "*Condition 1*" is identified. Thus, if "*Condition 1*" classifies the fault as CG or ABG fault, and "*Condition 2*" classifies it as AG fault, the final faulted phase identification provided by the algorithm will be the ABG fault.

If the fault cannot be classified as an "*Earth fault*", the next step is to check if the fault is a "*Line-to-Line fault*" by comparing the voltages measured by the relay in positive and negative sequence with a threshold setting. A "*Line-to-Line fault*" is expected if this threshold is exceeded. The result will be "*AB fault*" if the phase shift between $V_{A2}$ and $V_{A1}$ is in the range from 180° to 300°, "*BC fault*" if the phase ranging from 300° to 60°, or "*CA fault*" when the phase shift goes from 60° to 180°.

If the thresholds for declaring a fault as "*Earth fault*" or "*Line to Line fault*" are not exceeded, the fault is classified as a "*Three-phase fault*".

It must be considered that the implemented *FPSA4* is an adaptation of the described in [6]. During the algorithm operation analysis, some limitations were found. For example, it does not detect open pole scenarios, and in case of resistive faults, when the angle falls close to the angle limits, the selection fails. Furthermore, like *FPSA2*, the algorithm operation must be blocked in case of fuse failure. Consequently, the algorithm must be combined with others to provide a reliable faulted phase selection.

## 4. Proposed multicriteria FPS algorithm (M-FPSA)

The FPS algorithms described previously have advantages, but they are not valid for all the scenarios that can occur in the electrical power system. This section describes the different criteria (known as quality criteria) used to provide reliability to the selection supplied by each

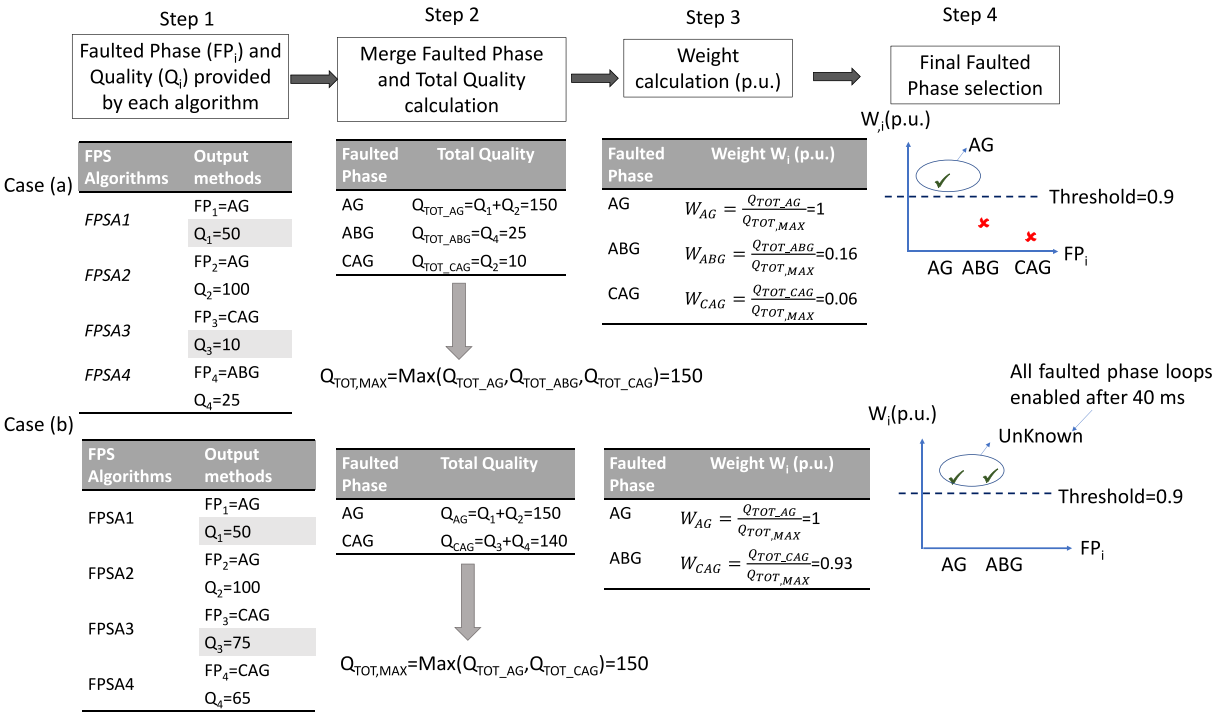


**Fig. 10.** Example of operation of the Proposed M-FPSA.

algorithm in each event and obtain the final faulted phase selection by the *M-FPSA*. For each event, the algorithms with higher quality value will have more weight and therefore have more reliability.

### 4.1. Quality criteria used for each of the faulted phase selection algorithms

Quality criteria give more importance to algorithms with higher reliability according to different parameters during each event. The higher the quality value associated, the greater the reliability of the selection and greater influence in the final faulted phase selection.

The quality criteria selection is based on the performance of electrical magnitudes measured during the fault. The selection of these electrical parameters and the evaluation of how their performance affects the faulted phase selection quality is empirically determined by analyzing the FPS algorithm's performance in laboratory tests.

The first step in the quality criteria definition is to evaluate how the different generation scenarios, fault types, fault location and fault resistances affect the electrical magnitudes performance used to determine the faulted phase in each algorithm. With this information, the design parameter values ($\beta_{Mi,j}$) in which the quality criteria change can be obtained.

Once this information is known, the next step consists of analyzing how the different quality values (0, 25, 50, 75 and 100 %) assigned to each $\beta_{Mi,j}$ interval affect the success of the *FP* selection provided by each algorithm. From the analysis of the FPS performance in the different scenarios, the quality values are assigned to maximize their success index.

Fig. 9 summarizes the selected quality criteria, where $\beta_{Mi,j}$ are design parameters defined during the analysis stage of electrical magnitudes performance.

As explained in Section 3.1.1, *FPSA1* is based on superimposed sequence currents. The quality criterion in this algorithm ($Q_1$) depends on the zero-sequence current ($I_0$) magnitude measured during the fault. As shown in Fig. 9 (a), the $Q_1$ value is obtained by comparing the $I_0$ measured value with the design parameters ($\beta_{M1,1}$, $\beta_{M1,2}$) defined during the analysis stage of *FPSA1*. For example, if $I_0$ is less than $\beta_{M1,1}$ or higher than $\beta_{M1,2}$, $Q_1$ will be 50. By contrast, if $I_0$ is in the range of ($\beta_{M1,1}$, $\beta_{M1,2}$), $Q_1$ will be 75.

*FPSA2* is based on the superimposed sequence voltages, as described in Section 3.1.2. As shown in Fig. 9 (b), the quality criterion value ($Q_{Alg\_2}$) depends on incremental voltage variations during the fault: the more significant the incremental voltage, the better reliability of the FP provided by this algorithm is.

*FPSA3* considers the phase angle difference between negative sequence current ($I_{A2}$) and zero-sequence current ($I_{A0}$), as summarized in Section 3.2.1. In this case, the quality criterion ($Q_3$) depends on the minimum value between the zero-sequence current ($I_0$) and the negative-sequence current ($I_2$) magnitude measured during the fault, as indicated in Fig. 9 (c). This value is compared with four design parameters ($\beta_{M3,1}$, $\beta_{M3,2}$, $\beta_{M3,3}$ and $\beta_{M3,4}$). Fig. 9 (c) shows that $Q_{Alg\_3}$ increases with the minimum between $I_0$ and $I_2$.

Finally, *FPSA4* is based on voltage phasors, as described in Section 3.2.2. In this case, the quality criterion ($Q_4$) depends on the ratio between the negative and the positive sequence voltage ($V_2/V_1$) and the relationship between the negative-sequence current ($I_2$) and positive-sequence current ($I_1$) magnitude, as it is shown in Fig. 9 (d). The value of $I_2$ defines two different curves. The blue line defines the quality criterion ($Q_4$) if $I_2$ is higher than 10 % of $I_1$. By contrast, the orange line is used if $I_2$ is less than this threshold. For both cases, the same design parameters ($\beta_{M4,1}$, $\beta_{M4,2}$, $\beta_{M4,3}$ and $\beta_{M4,4}$) are used to obtain $Q_4$.

Once the quality values ($Q_1$, $Q_2$, $Q_3$ and $Q_4$) are obtained and before their evaluation in the *M-FPSA*, an additional factor is applied to each algorithm. This new factor represents the effect of the strength of the source behind the relay location in the faulted phase selection quality. For example, it is known that algorithms based on current values do not behave correctly when fault current comes from unconventional sources such as PV plants or type-IV wind turbines or when weak infeed conditions are present. In these scenarios, algorithms based on voltages are prioritized before algorithms based on currents to increase the reliability of the final faulted phase selection because they are more reliable before weak sources.

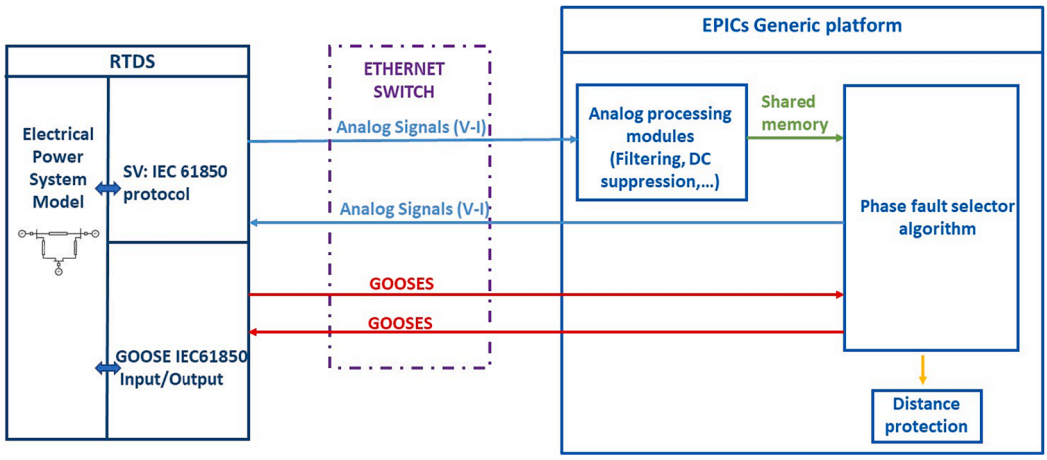


**Fig. 11.** General diagram of laboratory test bench.

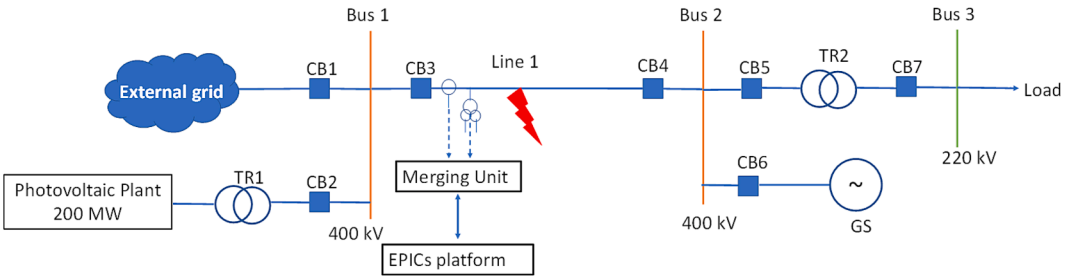


**Fig. 12.** Test network used to analyze the M-FPSA.

**Table 1**
Circuit breaker status for each scenario.

| Grid configuration | CB1 | CB2 | CB3 | CB4 | CB5 | CB6 | CB7 |
|---|---|---|---|---|---|---|---|
| Scenario 1 (SIR = 0.5 and SIR = 5) | Closed | Opened | Closed | Closed | Opened | Closed | Closed |
| Scenario 2 (SIR = 0.5) | Closed | Opened | Closed | Closed | Closed | Opened | Closed |
| Scenario 3 (SIR = 0.5) | Opened | Closed | Closed | Closed | Opened | Closed | Closed |

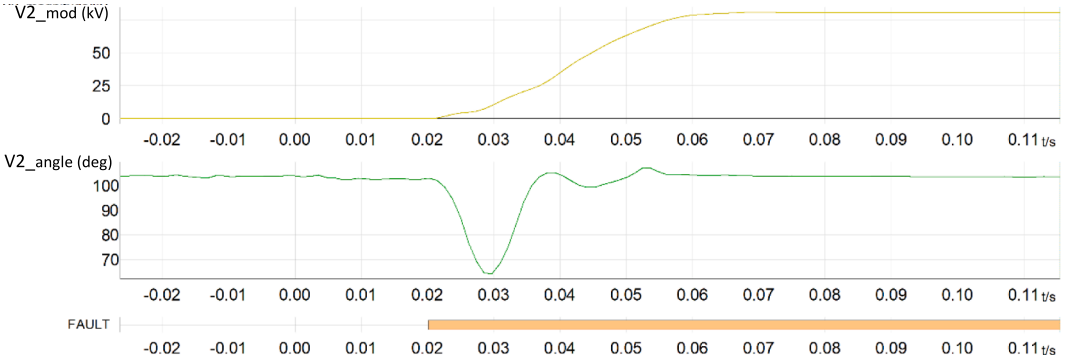


**Fig. 13.** Transient signal during a resistive fault.

### *4.2. Proposed multicriteria FPS algorithm description used for the final faulted phase selection*

Once faulted phase and quality values are obtained from the different FPS algorithms under study ($FP_i$ and $Q_i$, respectively), a final step is needed to carry out the final faulted phase selection. It consists of making a final weighting calculation to obtain the faulted phase. This task is illustrated in Fig. 10 through two examples.

In the first step, the four FPS algorithms explained in Section 3 provide four results for the faulted phase ($FP_1$, $FP_2$, $FP_3$ and $FP_4$) and four quality values ($Q_1$, $Q_2$, $Q_3$ and $Q_4$). In the second step, all the qualities obtained from the algorithms in Step 1 that give the same FP are added, resulting in several possible faulted phase selections with different total quality values ($Q_{TOT\_i}$). For example, as shown in Case (a) from Fig. 10, the algorithms *FPSA1* and *FPSA2* are providing the same faulted phase selection ($FP_1 = FP_2 =$ AG), then their qualities ($Q_1 = 50$, $Q_2 = 100$) are added obtaining the total quality $Q_{TOT\_AG}$ of 150. Furthermore in this step, the FPs obtained are sorted in descending order of their quality

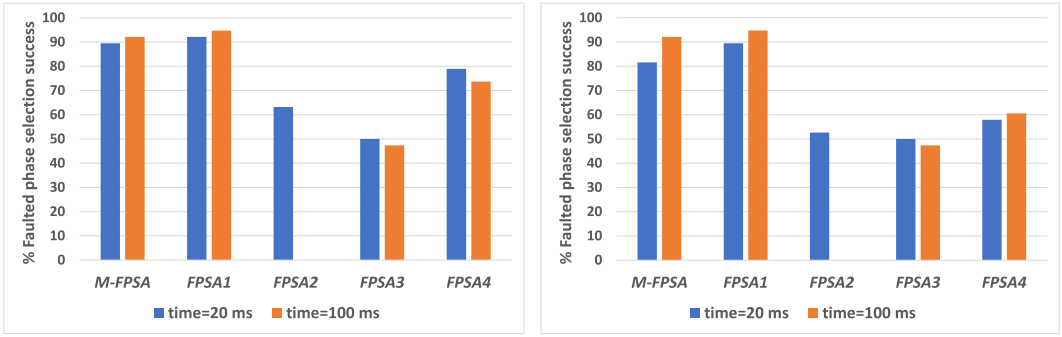


**Fig. 14.** Faulted phase selection-Scenario 1: Short line (a) Forward direction (b) Reverse direction.

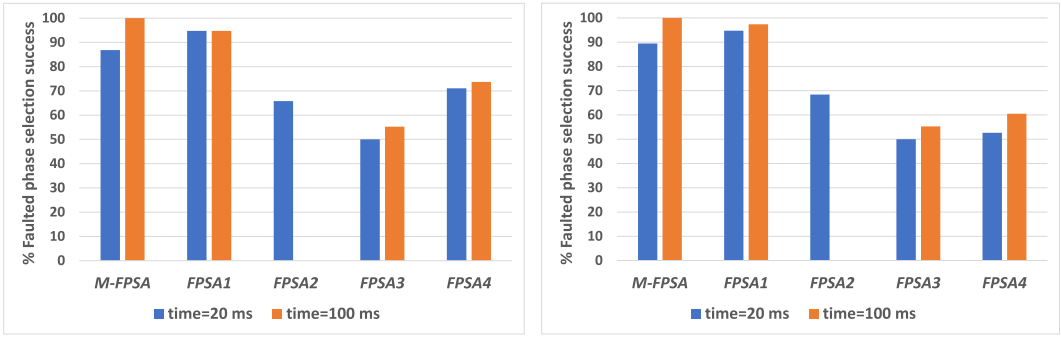


**Fig. 15.** Faulted phase selection-Scenario 1: Long line (a) Forward direction (b) Reverse direction.

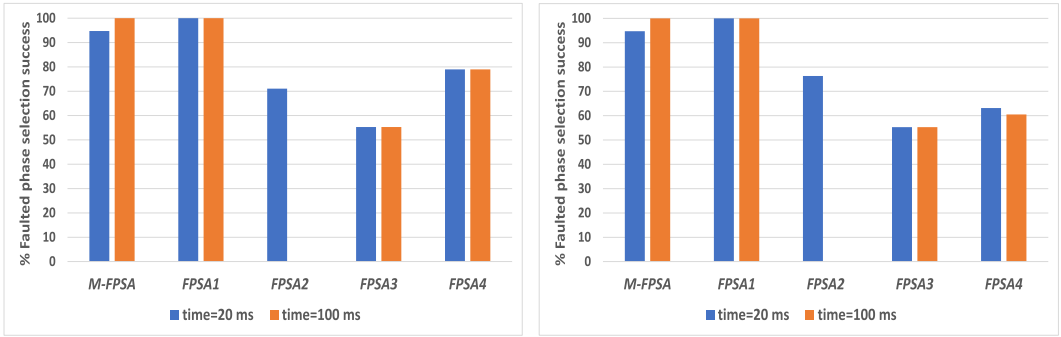


**Fig. 16.** Faulted phase selection-Scenario 2 (a) Forward direction (b) Reverse direction.

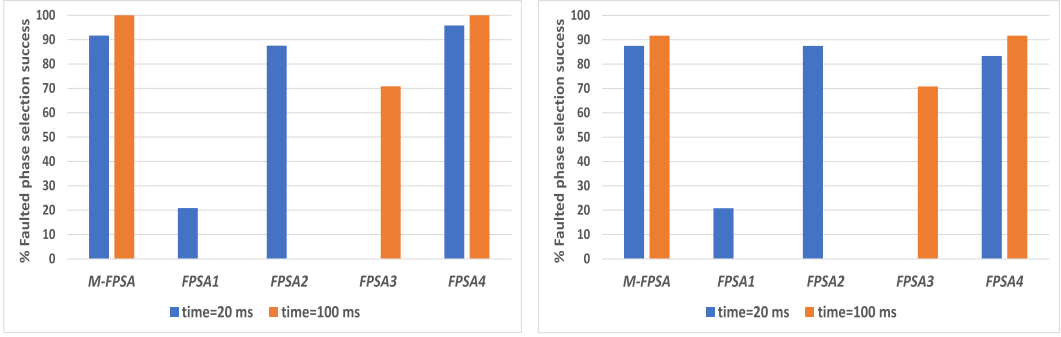


**Fig. 17.** Faulted phase selection-Scenario 3 (a) Forward direction (b) Reverse direction.

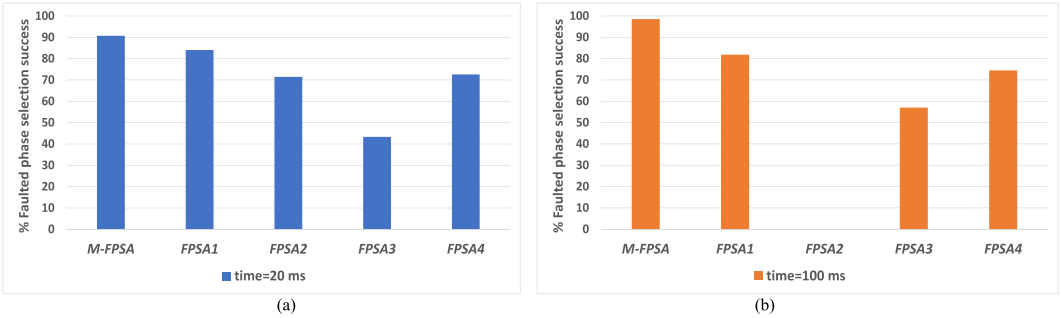


**Fig. 18.** Faulted phase selection: Global results: (a) Time instant = 20 ms (b) Time instant = 100 ms.

**Table 2**
Generator data.

| Generator data | Thevenin equivalent | Synchronous generation |
|---|---|---|
| Nominal Voltage (kV) | 400 | 400 |
| Phase (deg) | 10 | 0 |
| Frequency (Hz) | 50 | 50 |
| Resistance Series + (Ohm) | 0.05 | 0.05 |
| Resistance Parallel + (Ohm) | 1E38 | 1E38 |
| Inductance 1 Parallel (Henry) | 3.18e-2 | 3.18e-2 |
| Resistance 0 Series (Ohm) | 3 | 3 |
| Inductance 0 Series (Ohm) | 9.55e-2 | 9.55e-2 |

**Table 3**
Transmission line.

| Line 1 | |
|---|---|
| Model | Bergeron (RLC) |
| Positive Sequence Series Resistance (Ohm/km) | 0.0271 |
| Positive Sequence Series Ind. Reactance (Ohm/km) | 0.2785 |
| Positive Sequence shunt Cap. Reactance (MOhm*km) | 0.2429 |
| Zero Sequence Series Resistance (Ohm/km) | 0.1960 |
| Zero Sequence Series Ind. Reactance (Ohm/km) | 0.8239 |
| Zero Sequence Shunt Cap. Reactance (MOhm*km) | 0.4137 |

**Table 4**
Power transformer.

| Power transformer | TR1 | TR2 |
|---|---|---|
| Transformer rating(3 Phase) (MVA) | 225 | 200 |
| Winding #1 Connection | Wye | Delta |
| Winding #2 Connection | Delta | Wye |
| Base frequency (Hz) | 50 | 50 |
| Base primary voltage (L-L RMS) (kV) | 400 | 400 |
| Base secondary voltage (L-L RMS) (kV) | 14.5 | 220 |
| Leakage inductance of Tx (p.u.) | 0.15 | 0.104 |
| No load losses (p.u.) | 0.001 | 0.00048 |
| Winding 1 Magnetizing current (%) | 1 | 1 |
| Winding 2 Magnetizing current (%) | 1 | 1 |

values ($Q_{TOT\_AG} > Q_{TOT\_ABG} > Q_{TOT\_CAG}$) and the maximum quality value is obtained ($Q_{TOT,MAX} = Max(Q_{TOT\_AG}, Q_{TOT\_ABG}, Q_{TOT\_CAG})$). In the third step, the quantities $Q_{TOT\_i}$ are normalized using as a base the maximum value of the qualities obtained in Step 2 ($Q_{TOT,MAX}$). In the last step (Step 4), the normalized values ($W_i$) from Step 3 are compared with a threshold experimentally defined (0.9p.u.). This threshold makes identifying faulted phase selections with non-significant quality differences possible. If only one FP has a normalized value higher than the threshold, it would be selected as the final faulted phase, as shown in Case (a) from Fig. 10. By contrast, if there are several faulted phases whose normalized value is higher than the threshold, the final faulted phase will be identified as *Unknown* because several faulted phase selections with similar total quality are available and cannot be distinguished. Therefore, all impedance loops are released after a pre-set time, as in the example from Fig. 10 (b).

## 5. Laboratory test bench

This section describes the laboratory test bench used to check the proposed *M-FPSA*. The laboratory includes an EPICS platform implemented over a server Lenovo SE350 with Rocky Linux 8.5 operating system with 16 cores (2.2 GHz each one) and 64 GB of RAM, a communications switch (Hirschmann Greyhound GRS1042), and an RTDS simulator including four giga-transceiver network communication version 2 (GTNETx2) cards and one giga-transceiver network communication (GTNET) card able to work with IEC61850 Sampled Values and IEC 61850 GOOSE. All these elements are integrated into an infrastructure able to emulate and test any scenario in the grid.

Fig. 11 displays a diagram of the laboratory test bench. In this setup, it is possible to use RTDS to model electrical power systems that interact through hardware in the loop simulations, using real equipment, control systems, and electrical protection schemes. Therefore, it is a very convenient setup to test EPICS platform services and algorithms before their implementation in the field.

The RTDS allows the simulation of electrical power systems in real-time. The GTNETx2 card can be programmed with the IEC61850 SV firmware (GTNETx2_SV) or with the IEC61850 GOOSE firmware (GTNETx2_GSE).

Using GTNETx2_SV firmware, it is possible to convert signals, as voltages and currents generated in real-time, into IEC61850 SV signals that the EPICS platform can subscribe. In this study, the standard IEC61850-9-2 LE [27] was used for SV publications made by the RTDS. Moreover, using the GTNETx2_SV firmware, it is possible to subscribe to IEC61850 SV signals published by the EPICS platform, which can send some feedback signals useful for analyzing the behavior of the service or algorithm under test.

Using the GTNETx2_GSE firmware, it is possible to publish GOOSE messages with the information needed by the service under test processed by EPICS and with that firmware, it is also possible to subscribe to GOOSE messages published by the EPICS to complete the hardware in the loop (HIL) platform.

The EPICS works as a generic platform where different algorithms can be developed and implemented using any programing language. In this study C++ [28] has been selected. The resulting outputs of the algorithms are communicated via IEC61850 GOOSE messages or IEC61850 SV to the RTDS that execute the remedial actions in real time over the simulated electrical power system.

All the communications inside the laboratory test bench pass through the Ethernet switch Hirschmann GRS1042. An additional computer is used to program and configure all the elements inside the laboratory.

## 6. Test network

This section describes the test network used to analyze the M-FPSA

and the implemented faulted phase selection algorithms. In the grid transmission model described in Fig. 12, the external grid is represented by a 400 kV Thevenin equivalent with solid grounded connection. This external grid is connected to a 200 MVA load (with a power factor of 0.85) through an overhead line and a 400/220 kV power transformer (TR2). A 200 MW photovoltaic power plant (PV) model with a grid following control based on decoupled control strategy has also been connected at Bus 1 to evaluate the behavior of the algorithms under weak infeed. The PV control model includes the fault-ride-through and fast fault current injection requirements defined in the Spanish Grid Code for Type D power park modules [29,30]. Furthermore, a current injection strategy that prioritizes the positive and negative sequence reactive current injection concerning the positive sequence active current injection has been used during this study, as described in [22]. Finally, a synchronous generation (GS) is connected to Bus 2.

The electrical data from generators, power transformers, and the transmission line can be found in Appendix A.

The study considers the following three scenarios:

- Scenario 1: Strong grid in the local and remote terminal. Two-line lengths (long line (SIR = 0.5) and short line (SIR = 5)) are tested in this scenario.
- Scenario 2: Strong grid in the local terminal and weak grid from the load in the remote terminal. Long line is tested in this scenario (SIR = 0.5).
- Scenario 3: Weak grid from the PV power plant in the local terminal and strong grid in the remote terminal. Long line is tested in this scenario (SIR = 0.5).

To generate the previous scenarios, the circuit breakers shown in Fig. 12 are operated as detailed in Table 1.

Furthermore, the following fault types are applied at 2 %, 50 % and 97 % of Line 1 in Forward and reverse directions for each scenario:

- Single line-to-ground faults: AG, BG and CG
- Line-to-line faults: AB, BC and CA
- Line-to-line to ground faults: ABG, BCG and CAG
- Three-phase fault: ABC
- Evolving faults (only at 50 % of Line 1): AG → ABG, BG → BCG and CG → CAG
- Switch onto fault (only at 2 % and 97 %): AG, BC, CAG and ABC

Consequently, the study has carried out 270 tests, also including resistive faults. The definition of fault resistance in protection studies is not straightforward because it is highly variable and relatively unknown [31]. The study described in [32], where the authors process real faults' data on 400 kV lines, concludes that the typical fault resistance is below 10 Ω in 92 % of the analyzed faults. Furthermore, the IEC 60255-121 standard [33], where the functional requirements of distance protection are specified, sets a cover resistance of 15 Ω for the line-to-ground faults and 10 Ω for the line-to-line faults. According to the values found in the literature, the following fault resistance values were considered during tests: 0.01 Ω, 10 Ω and 15 Ω. Fault resistances with higher values have not been considered for two reasons: first, they are not very frequent, and second, they are difficult to detect by many protection algorithms. There are specific methods for those cases that have not been included in the analysis.

## 7. Test results and discussion

This section compares the faulted phase success achieved by each of the four algorithms separately and the *M-FPSA* proposed in this article when tested in the scenarios described in Section 6.

In the analyzed tests, an unsuccessful selection means that the FPSA cannot provide a clear selection (provides *NONE*), or the result is a wrong selection.

The FPS algorithms used during the study are based on the calculation of phasors. These phasors are provided by Fourier transform (FT) applied to the voltage and current signals. The FT usually needs a full cycle to provide relevant results. However, the voltage and current signals must reach a stable value to obtain proper results. During tests, it is observed that there are fault scenarios where transient signals need more than a cycle to achieve a steady state. For example, Fig. 13 shows the magnitude and angle of negative sequence voltage (V2_mod and V2_angle, respectively) measured during a resistive fault. As is shown in the figure, the transient signals need around 30 ms to reach a stable state.

Furthermore, grid codes, such as the Spanish Grid Code, allow for a renewable resources time response of up to 80 ms [30]. Additionally, FPS algorithms are used by protection functions such as distance protection for its operation. Distance protection not only operates instantaneously (Zone 1). It also works with time delays (such as Zone 2 or 3). The time delays reach more than 100 ms. Then, the faulted phase selection algorithm must be stable over time to ensure the correct operation of distance protection considering these time delays.

For all these reasons, FPS algorithms are evaluated in two instants regarding the fault inception: at time = 20 ms (Transient state) and at time = 100 ms (Steady-State). All in all, it must be indicated that although the *M-FPSA* test results are shown at 100 ms, it does not mean that the algorithm needs this time to obtain the successful faulted phase selection. The *M-FPSA* provides the same proper phase selection at a time below 30 ms that is considered suitable for instantaneous protection functions operation.

Next figures summarize test results described in Section 6. They show that the success of each algorithm varies with the fault direction (forward or reverse) and the grid configuration (grid scenarios). For example, *FPSA1* behaves correctly when conventional sources supply fault current (Figs. 14–16). Still, the success when unconventional sources supply the fault current is low because it cannot obtain the proper selection (see Fig. 17). Furthermore, this algorithm is less sensitive to the grid configuration, providing good results independently of the SIR.

When *FPSA2* is used, figures show better behavior when evaluated at 20 ms than at 100 ms after the fault inception. This method is based on incremental values without memory and therefore, after one cycle, the incremental value comes to zero. Furthermore, its better performance is reached when unconventional sources are connected (success selection = 88 %). Moreover, the results obtained when directionality changes are very similar.

*FPSA3* is suitable only for faults involving ground connection so that the percentage of success is reduced compared with the other methods that can select all fault types. Besides, the figures show that it behaves better in grid configuration with less SIR value (SIR = 0.5). When unconventional sources are connected, it cannot select the faulted phase selection at 20 ms but provides good results at 100 ms. Moreover, as in *FPSA2*, the results obtained when directionality changes are very similar.

*FPSA4* is more sensitive to the directionality, improving the performance with forward direction. Furthermore, it behaves better in short lines and provides outstanding results when unconventional sources are connected to the grid.

Finally, *M-FPSA* shows very good results in all scenarios. This algorithm provides suitable faulted phase selections under conventional and unconventional sources and when faults are applied in forward and reverse directions.

Slight differences between the success rate of the algorithms' performance in the transient state (20 ms) vs the steady-state (100 ms) can be observed in the figures (Figs. 14–17). These differences (up to 10 % for individual algorithms) are introduced during resistive faults, and they are caused by the following two factors: a) the fault dynamic during a resistive fault is slow and it needs a bit more than 20 ms to reach a stable state; this affects all the methods; b) the angle criteria used to

select the faulted phase fall close to the limits of the angle section; this only affects *FPSA3* and *FPSA 4* algorithms.

As shown in the previous figures (Figs. 14–17), the four algorithms have strengths and weaknesses, and their behavior worsens in one or several analyzed scenarios. However, *M-FPSA* provides a success percentage higher than 90 % in steady-state fault for all scenarios.

Fig. 18 summarizes the success of the faulted phase selection provided by each algorithm considering all scenarios to have a global vision of their performance. From Fig. 18, it is concluded that the *M-FPSA* improves the faulted phase selection when it is evaluated in transient and in steady-state fault conditions (20 ms and100 ms after the fault inception, respectively).

Considering that the renewable penetration level will increase during the next years, *FPSA1* will reduce its reliability. Still, the *M-FPSA* will work properly during the transient period, as it is demonstrated in Fig. 17.

## 8. Conclusions

The substation digitalization provides new tools to improve the protection system behavior. With this aim, this article proposes and develops a novel *Multicriteria Faulted Phase Selection Algorithm (M-FPSA)* that enhances the faulted phase selection provided by algorithms usually used in commercial protection relays. Four FPS algorithms have been assessed in this study. Two of these algorithms are proposed and developed during this study. They are based on superimposed sequence components theory. The other two algorithms are adapted from the literature review. All these algorithms are implemented in EPICS platform, which is already installed in a real substation. EPICS platform allows making software independent from hardware, improving protection and control systems reliability, flexibility, and adaptability. From a research point of view, this platform is a tool for testing new protection solutions in a real environment of fully digital substations.

In the novel *M-FPSA*, quality criteria are defined to provide reliability to the faulted phase selection supplied by each FPS algorithm, improving the performance of faulted phase selectors in scenarios that typically occur in transmission power grids.

Several tests have been carried out in different grid configurations (long line, short line, weak grid and unconventional sources) to identify the strengths and weaknesses of the four algorithms, define quality criteria and evaluate the performance of *M-FPSA*.

The test results conclude that the success of the faulted phase selection provided by each algorithm varies with the fault direction (forward or reverse) and the grid configuration. However, globally, when all the scenarios are considered, the *M-FPSA* performs better. For example, *FPSA1* behaves accurately when conventional sources supply fault current but is not suitable with unconventional sources because it cannot correctly select faulted phases. Furthermore, *FPSA2* or *FPSA3* are insensitive to the fault direction, but the success of these algorithms are less than in *FPSA1*. *FPSA4* behavior depends on the scenario, providing better results when applied in short lines.

When the *M-FPSA* is tested under the same scenarios, it shows that the success is higher than 90 % in steady state fault for every analysed scenario, reaching almost 100 % in most cases. Then, the multicriteria approach presents higher reliability, regardless of the grid configuration and fault type. This fact makes this approach more accurate than the independent algorithms because its success rate is not subjected to aspects such as the fault direction, the line length or the strength of the source that provides the fault current.

The following steps in the development of *M-FPSA* will include test scenarios with different grounded topologies, such as ungrounded and grounded with impedance, to analyze the best combination for distribution systems.

## CRediT authorship contribution statement

**María Teresa Villén Martínez:** Conceptualization, Methodology, Validation, Software, Writing – review & editing. **Maria Paz Comech:** Writing – review & editing. **Anibal Antonio Prada Hurtado:** Conceptualization, Methodology, Validation, Software, Writing – review & editing. **Miguel Angel Olivan:** Software, Validation. **Carlos Rodriguez del Castillo:** Conceptualization, Methodology. **David López Cortón:** Conceptualization, Methodology, Validation. **Rubén Andrino Gallego:** Conceptualization, Methodology.

## Declaration of Competing Interest

The authors declare that they have no known competing financial interests or personal relationships that could have appeared to influence the work reported in this paper.

## Data availability

The data that has been used is confidential.

## Acknowledgements

The EPICS (Edge Protection and Intelligent Control System) project of ELEWIT (A REDEIA company), which has allowed the use of the EPICS platform for the development and testing of a faulted phase selection algorithm based on weight criterion.

## Appendix A

In this section, it is described the grid parameters used during the study (see Tables 2–4).

## References

[1] Ziegler G. Numerical distance protection: principles and applications. 4th edition. John Wiley & Sons; 2011.
[2] Huang S, Luo L, Cao K. A novel method of ground fault phase selection in weak-infeed side. IEEE Trans Power Deliv 2014;29(5):2215–22. https://doi.org/10.1109/TPWRD.2014.2322073.
[3] Song G, Wang C, Wang T, Kheshti M, Kang X. A phase selection method for wind power integration system using phase voltage waveform correlation. IEEE Trans Power Deliv 2017;32(2):740–8. https://doi.org/10.1109/TPWRD.2016.2577890.
[4] Huang SF, Chen ZH, Zhang YP, Bi TS. Adaptive residual current compensation for robust fault-type selection in mho elements. IEEE Trans Power Deliv 2005;20(2):573–8. https://doi.org/10.1109/TPWRD.2005.844354.
[5] Noori MR, Shahrtash SM. Combined fault detector and faulted phase selector for transmission lines based on adaptive cumulative sum method. IEEE Trans Power Deliv 2013;28(3):1779–87. https://doi.org/10.1109/TPWRD.2013.2261563.
[6] Price E, Einarsson T. The performance of faulted phase selectors used in transmission line distance applications. In: 2008 61st annual conference for protective relay engineers; Apr. 2008. p. 484–90. doi: 10.1109/CPRE.2008.4515074.
[7] Costello D, Zimmerman K. Determining the faulted phase. In: 2010 63rd annual conference for protective relay engineers; Mar. 2010. p. 1–20. doi: 10.1109/CPRE.2010.5469523.
[8] Dong X, Kong W, Cui T. Fault classification and faulted-phase selection based on the initial current traveling wave. IEEE Trans Power Deliv 2009;24(2):552–9. https://doi.org/10.1109/TPWRD.2008.921144.
[9] Lin X-N, Zhao M, Alymann K, Liu P. Novel design of a fast phase selector using correlation analysis. IEEE Trans Power Deliv 2005;20(2):1283–90. https://doi.org/10.1109/TPWRD.2004.834298.
[10] Li W, Bi T, Yang Q. Study on sequence component based fault phase selector during power swings. In: 2010 5th International conference on critical infrastructure (CRIS); Sep. 2010. p. 1–5. doi: 10.1109/CRIS.2010.5617576.
[11] Bo ZQ, Aggarwal RK, Johns AT, Li HY, Song YH. A new approach to phase selection using fault generated high frequency noise and neural networks. IEEE Trans Power Deliv 1997;12(1):106–15. https://doi.org/10.1109/61.568230.
[12] Deng X, Yin X, Zhang Z, Kong X, Qiu C. A novel fault phase selector for double-circuit. Transmission Lines 2012;10(7). https://doi.org/10.11591/TELKOMNIKA.V10I7.1569.
[13] Wang X, et al. A phase selection element for high resistance ground faults of transmission line. IEEE Power Energy Soc Gen Meet (PESGM) 2019;2019:1–4. https://doi.org/10.1109/PESGM40551.2019.8974123.

[14] Espinoza RF, Dias O, Tavares MC, Molina YP. Application of a robust faulted phase selector to high-resistance and weak-infeed fault conditions on a 1000-kV UHV transmission line. Electric Power Syst Res 2021;197:107244. https://doi.org/10.1016/j.epsr.2021.107244.
[15] Liu Z, Gao H, Luo S. A fault phase and line selection method of doublecircuit transmission line on the same tower based on transient component. In: 2019 IEEE 8th international conference on advanced power system automation and protection (APAP); Oct. 2019. p. 1058–62. doi: 10.1109/APAP47170.2019.9225091.
[16] Huang S, Luo L, Cao K. A novel method of ground fault phase selection in weak-infeed side. IEEE Trans Power Deliv 2014;29(5):2215–22. https://doi.org/10.1109/TPWRD.2014.2322073.
[17] Plataforma EPICS: implementación flexible y escalable de sistemas automáticos. ELEWIT. https://www.elewit.ventures/index.php/es/actualidad/plataforma-epics-implementacion-flexible-y-escalable-de-sistemas-automaticos (accessed Jul. 08, 2022).
[18] RTDS Technologies. Real time digital simulator (RTDS). https://www.rtds.com/(accessed Feb. 10, 2022).
[19] Rudevz U, Osredkar P, Mihali R. Overcurrent protection-relay testing with Real-Time Digital Simulator Hardware; 2012.
[20] Moravej Z, Bagheri S. Testing of differential relay operation for power transformers protection using RTDS. In: 2015 30th international power system conference (PSC); 2015. p. 99–105.
[21] Prada Hurtado AA et al. Application of IIA method and virtual bus theory for backup protection of a zone using PMU data in a WAMPAC system. Energies 2022; 15(9). doi: 10.3390/en15093470.
[22] Villén MT et al. Influence of negative sequence injection strategies on faulted phase selector performance. Energies 2022;15(16). doi: 10.3390/en15166018.
[23] UCA International Users Group. IEC 61850-9-2LE (light edition) implementation guideline for digital interface to instrument transformers using IEC 61850-9-2. [Online]. Available: www.ucainternational.org.
[24] Apostolov AP, Tholomier D, Richards SH. Superimposed components based sub-cycle protection of transmission lines. In: IEEE PES power systems conference and exposition, 2004. Vol. 1; Oct. 2004. p. 592–7. doi: 10.1109/PSCE.2004.1397508.
[25] Horton P, Swain S. Using superimposed principles (Delta) in protection techniques in an increasingly challenging power network. In: 2017 70th annual conference for protective relay engineers (CPRE); Apr. 2017. p. 1–12. doi: 10.1109/CPRE.2017.8090059.
[26] Opoku K, Pokharel S, Dimitrovski A. Superimposed sequence components for microgrid protection: a review. In: 2022 IEEE Texas power and energy conference (TPEC), College Station, TX, USA; Feb. 2022. p. 1–6. doi: 10.1109/TPEC54980.2022.9750756.
[27] IEC 61850-9-2 Communication networks and systems in substations – Part 9-2: specific communication service mapping (SCSM) –sampled values over ISO/IEC 8802-3.
[28] Stroustrup B. The C++ programming language. Pearson Education; 2013.
[29] Ministerio para la Transición Ecológica y el Reto Demográfico. Real Decreto 647/2020, de 7 de julio, por el que se regulan aspectos necesarios para la implementación de los códigos de red de conexión de determinadas instalaciones eléctricas, vol. BOE-A-2020-7439; 2020. p. 48722–57. [Online]. Available: https://www.boe.es/eli/es/rd/2020/07/07/647.
[30] Ministerio para la Transición Ecológica y el Reto Demográfico, Orden TED/749/2020, de 16 de julio, por la que se establecen los requisitos técnicos para la conexión a la red necesarios para la implementación de los códigos de red de conexión, vol. BOE-A-2020-8965; 2020. p. 62406–58. [Online]. Available: https://www.boe.es/eli/es/o/2020/07/16/ted749.
[31] Blackburn JL. Symmetrical components for power systems engineering. New York, NY, USA: CRC Press; 1993.
[32] Sorrentino E, Ayala C. Measurement of fault resistance in transmission lines by using recorded signals at both ends. Electric Power Syst Res 2016;140:116–20.
[33] IEC 60255-121. Measuring relays and protection equipment-part 121: functional requirements for distance protection; 2014.